

Article

Dynamic High-Type Interval Type-2 Fuzzy Logic Control for Photoelectric Tracking System

Shuwang Qin ^{1,2,3} , Chao Zhang ^{1,2,3,*}, Tao Zhao ⁴, Wei Tong ⁴, Qiliang Bao ^{1,2,3} and Yao Mao ^{1,2,3} 

¹ Key Laboratory of Optical Engineering, Chinese Academy of Sciences, Chengdu 610209, China; mrqtian@126.com (S.Q.); control@ioe.ac.cn (Q.B.); maoyao@ioe.ac.cn (Y.M.)

² Institute of Optics and Electronics, Chinese Academy of Sciences, Chengdu 610209, China

³ University of Chinese Academy of Sciences, Beijing 100049, China

⁴ College of Electrical Engineering, Sichuan University, Chengdu 610065, China; zhaotaozhaogang@126.com (T.Z.); tongwei@stu.scu.edu.cn (W.T.)

* Correspondence: zhangchao@ioe.ac.cn

Abstract: This paper proposes a dynamic high-type control (DHTC) method based on an interval type-2 fuzzy logic controller (IT2FLC), which is used in the photoelectric tracking system to improve the steady-state accuracy and response speed. Adding integrators to the traditional multi-loop feedback control loop can increase the system type, thereby speeding up the response speed and improving the steady-state accuracy, but there is a risk of integral saturation. Switching the type dynamically according to the system state can avoid integral saturation while retaining the advantages of the high-type. Fuzzy logic control (FLC) can dynamically change the output value according to the input change and has the advantages of fast response speed and strong ability to handle uncertainties. Therefore, in this paper, the FLC is introduced into the high-type control system, and the output of the FLC is used as the gain of the integrator to control the on-off to achieve the goal of dynamic switching type, which is successfully verified in the experiment. IT2FLC introduces a three-dimensional membership function, which further improves the FLC's ability to handle uncertainties. From the experimental results, compared with T1FLC, IT2FLC's ability to handle uncertainties is significantly improved. In addition, in order to speed up the calculation speed of IT2FLC, this paper proposes an improved type-reduction algorithm, which is called weighted-trapezoidal Nie-Tan (WTNT). Compared with the traditional type-reduction algorithm, WTNT has faster calculation speed and better steady-state accuracy, and has been successfully applied to real-time control systems, which has good engineering application value. Finally, in order to reduce the interference of human factors and improve the automation level of the system, a multi-population genetic algorithm (MPGA) is used to iteratively optimize the parameters of the FLC, which improves the output accuracy. On the experimental platform of the flexible fast steering mirror (FFSM), the control effects of the traditional controller, T1FLC and IT2FLC are compared, which proves that the IT2FLC-DHTC system has a faster response performance, higher steady-state accuracy, and stronger ability to handle uncertainties.

Keywords: dynamic high-type control (DHTC); fuzzy logic control (FLC); interval type-2 fuzzy logic controller (IT2FLC); photoelectric tracking system; multi-population genetic algorithm (MPGA)



Citation: Qin, S.; Zhang, C.; Zhao, T.; Tong, W.; Bao, Q.; Mao, Y. Dynamic High-Type Interval Type-2 Fuzzy Logic Control for Photoelectric Tracking System. *Processes* **2022**, *10*, 562. <https://doi.org/10.3390/pr10030562>

Academic Editor: Jie Zhang

Received: 11 February 2022

Accepted: 1 March 2022

Published: 14 March 2022

Publisher's Note: MDPI stays neutral with regard to jurisdictional claims in published maps and institutional affiliations.



Copyright: © 2022 by the authors. Licensee MDPI, Basel, Switzerland. This article is an open access article distributed under the terms and conditions of the Creative Commons Attribution (CC BY) license (<https://creativecommons.org/licenses/by/4.0/>).

1. Introduction

Photoelectric servo tracking equipment is widely used in beam control systems, such as adaptive optics, free-space communication, line of sight stabilization, etc., and has important application value in military and civilian fields [1–3]. Its tracking performance is the most important index to evaluate the control system. Commonly used tracking control methods include PID [4,5], speed/acceleration lag compensation [6,7], and disturbance observer based on a multi-loop feedback control [8]. Among them, the PID method is simple in design, stable in performance, and the most widely used. However, due to its

slow dynamic response speed and low steady-state accuracy, it is difficult to adapt to the situation where the target volume becomes smaller, and the maneuverability becomes stronger in the current environment [9].

As early as the 1990s, the United States' Launch Area Theodolite System applied dynamic high-type control technology (DHTC), which has achieved great tracking accuracy and a wide range [10]. Dynamic high-type technology refers to dynamically connecting and disconnecting one or more integrators based on the original multi-loop feedback system to improve the response speed and steady-state accuracy while ensuring that the system does not have integral saturation. However, the research on DHTC in academia is still in its infancy. Tang constructed a PID-I system and added an integrator to the PID controller to achieve high-type control [1], and Papadopoulos et al. constructed the explicit analytical PID tuning rules for the design of type-III control loops based on the principle of the symmetrical optimum criterion [11], but they did not achieve the goal of changing the type in real time according to the system status, and there is a hidden danger of integral saturation. At present, in the research of dynamic high-type switching, the method of type switching relies on manual operation, and the switching moment will bring greater chattering to the system, which is far from meeting the needs of practical applications.

In recent years, the fuzzy logic control (FLC) method has developed rapidly, which provides a breakthrough for the realization of DHTC. As a rule-based nonlinear controller, the FLC provides a systematic method in which experts construct language information and transform it into a control strategy. It can solve many complex control problems that cannot be established for precise mathematical models. Therefore, FLC is an effective method to control uncertainties and inaccuracy in the system [12]. Later, researchers applied it to many practical systems in the control field. In [13], the two-level fuzzy feedback scheduling scheme is designed to adjust the task priority and period according to the combined effects of the response time and packet loss of cyber-physical systems for robot control, proving that fuzzy control has fast and accurate response performance in real-time systems. In [14], according to the characteristics of the actual reaction of the continuous stirred tank reactor, the T-S fuzzy model is used to study the problem of fault detection. In addition, the fuzzy controller is also used in the medical field, such as the fuzzy control-based energy aware routing protocol (EARP) applied in wireless body area networks (WBANs) [15] and combined with sliding mode control applied in gyroscope control systems [16,17]. In the study of DHTC, Qin et al. used T1FLC to construct the T1FLC-DHTC structure, which realized automatic switching of system types [18], but the control parameters of T1FLC completely relied on artificial settings, and in the real unstructured dynamic environment and many specific applications, the traditional T1FLC will face many uncertainties, mainly including measurement noise, friction, and rule base differences, etc. [19–22].

As an extension of the type-1 fuzzy logic system (T1FLS), the type-2 fuzzy logic system (T2FLS) was proposed. The feature of T2FLS is to fuzzify the membership value in the fuzzy set, which enhances the ambiguity of the set, thereby improving its ability to deal with uncertainties [23]. The experimental results show that in high uncertainties situations, T2FLS has significantly better performance than the corresponding T1FLS, and the higher the degree of uncertainties, the more obvious this advantage is [24]. The defuzzification process of T2FLC requires the use of type-reduction (TR) algorithms. Commonly used algorithms are EKM and EIASC based on iterative calculations [25–27], and NT algorithms that do not require iteration [28]. The TR algorithm based on iterative calculation has high calculation accuracy, but the calculation speed is slow; while algorithms such as NT that do not require iteration have fast calculation speed and sufficient accuracy to meet system requirements, so they are more suitable for real-time systems [29]. To further improve the speed and accuracy of the NT algorithm, this paper proposes a WTNT algorithm based on the principle of numerical integration. To reduce the dependence of the fuzzy controller on human experience, the multi-group genetic algorithm (MPGA) is used to optimize the FLC parameters.

The main contributions of this paper can be summarized as follows:

1. A DHT-IT2FLC system is constructed to realize dynamic high-type control. As a judging mechanism, the FLC changes the system type in real time according to the system status, which not only achieves the purpose of improving the steady-state accuracy and speeding up the response speed, but also avoids the hidden dangers of system oscillation and integral saturation caused by the increase of type.
2. Compared with the traditional controller and the T1FLC, the IT2FLC can significantly improve the ability of the system to handle uncertainty, make the system run more smoothly and stably, and enhance the robustness of the system.
3. Aiming at the TR problem of T2FLC in real-time system applications, the improved WTNT TR algorithm is proposed to reduce computational complexity. By comparison, WTNT has faster response speed and calculation accuracy than EKM and EIASC in this project.

The structure of this paper is as follows. Section 2 systematically introduces the background knowledge of DHTC, FLC, and MPGA; Section 3 introduces the design of the control system; Section 4 presents the experimental results, and make conclusions in Section 5.

2. Problem Formulation and Preliminaries

This chapter systematically introduces DHTC, FLC, and MPGA to prepare the basics for controller design.

2.1. DHTC

The commonly used photoelectric tracking control method is the classic type-I double closed-loop feedback control, as shown in Figure 1. In the figure, G_v is the mathematical model identified from the FSM experimental platform, and C_v is the speed controller. These two parts form an inner loop called the speed loop; the speed loop and the position controller C_p in the series form an outer loop called the position loop. The open-loop transfer function of the system is

$$G(s) = \frac{a \cdot k \cdot (T_3s + 1)}{s \cdot (T_4s + 1) \cdot (a + (T_1s + 1) \cdot (T_2s + 1))} = \frac{K \prod_{i=1}^m (\tau_i s + 1)}{s^v \prod_{j=1}^{n-v} (T_j s + 1)} \quad (1)$$

where a and k are the gains of the inner loop and the outer loop, respectively, and T_1 , T_2 , T_3 , and T_4 are the time constants of the transfer function of each controller. According to the definition in the principle of automatic control, since there is an integrator in the system, namely $v = 1$, it is a type-I system. The systematic error e is defined as

$$e(s) = r(s) - y(s) = (1 - \Phi(s))r(s) = E(s)r(s), \quad (2)$$

where r is reference input, y is systematic output, $E(s)$ is the error transfer function, $\Phi(s)$ is the closed-loop transfer function of the system

$$\Phi(s) = \frac{y(s)}{r(s)} = \frac{b_m s^m + b_{m-1} s^{m-1} + \dots + b_1 s + b_0}{a_n s^n + a_{n-1} s^{n-1} + \dots + a_1 s + a_0} \quad (3)$$

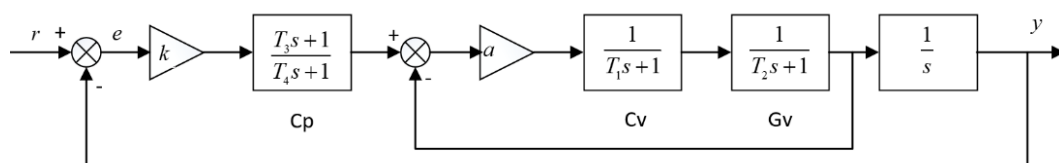


Figure 1. The classic type-I double closed-loop feedback system.

Therefore, $e(s)$ can be expressed as

$$e(s) = \frac{a_n s^n + \dots + c_m s^m + c_{m-1} s^{m-1} + \dots + c_1 s + c_0}{a_n s^n + a_{n-1} s^{n-1} + \dots + a_1 s + a_0} \tag{4}$$

where $c_i = (a_i - b_i), i = 0, \dots, m$. According to the final value theorem, when the system is in a stable state, the steady-state error $e(\infty)$ can be expressed as

$$e(\infty) = \lim_{s \rightarrow 0} \left(\frac{a_n s^n + \dots + c_m s^m + \dots + c_1 s + c_0}{a_n s^n + a_{n-1} s^{n-1} + \dots + a_1 s + a_0} \right) r(s) = \frac{\lim_{s \rightarrow 0} [s^{v+1} r(s)]}{K + \lim_{s \rightarrow 0} s^v} \tag{5}$$

The step signal, velocity signal, and acceleration signal existing in the physical system are expressed as $r(s) = \frac{R_1}{s}, r(s) = \frac{R_2}{s^2}, r(s) = \frac{R_3}{s^3}$. For the superimposed input of these three signals, $e(\infty)$ will remain in a certain range only when $v \geq 2$; that is, the system can reach a stable state only if the system type is greater than 2.

To improve the steady-state accuracy of the system, multiple integrators are added to the system to change the system into a high-type state. However, the increase of the system type will increase the step response overshoot and increase the system oscillation; as the gain of the integrator becomes larger, the oscillation will be greater, and in some extreme cases it will even reach the integral saturation state, causing the system to lose stability completely.

To solve the above-mentioned problems, the ‘dynamic high-type’ method was proposed. As shown in Figure 2, multiple integrators are connected in parallel in the forward path, and the on and off of the integrators are judged according to the system error state, and the type of the system is dynamically changed. However, there are two problems to be solved:

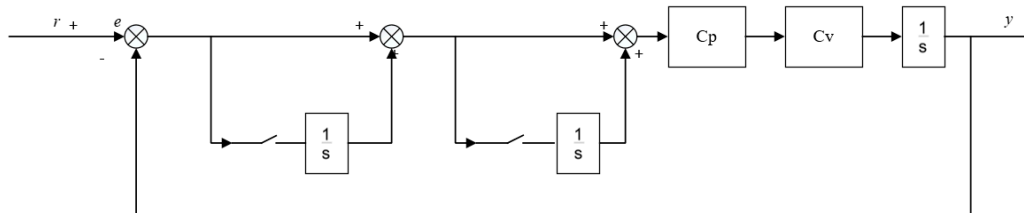


Figure 2. The DHTC structure diagram.

Question 1. The standard for type switching is not defined. When to increase the type and when to decrease it, no theoretical guidance is given in the current literature. Besides, the manual switching method used in most of the literature is inaccurate and not practical.

Question 2. The jitter caused by type switching is difficult to eliminate. In the existing research, every moment of type switching will bring greater jitter to the system, increase instability, and reduce its robustness.

2.2. IT2FLC

The common point of the T1FLS and T2FLS fuzzy systems is that they are based on the fuzzy rule library constructed by expert experience for fuzzy inference, and the input is processed to obtain the output. Generally, the structure of two inputs and one output is commonly used. The two inputs are the system error e and the error rate of change Δe , and the output is the control signal. The difference between the T1FLS and T2FLS lies in the membership function, defuzzification method, and the ability to deal with uncertainties.

2.2.1. Construct of IT2FLC

Let \tilde{A} be a type-2 fuzzy set (T2FS), $u \in [0, 1]$ is the primary membership degree of \tilde{A} , and $u' \in [0, 1]$ is the secondary membership degree of \tilde{A} . When u' is always 1, the

calculation amount of fuzzy inference can be greatly simplified. At this time, T2FLC is called interval T2FLC (IT2FLC). When $x \in X$ is input, \tilde{A} can be expressed by Equation (6):

$$\tilde{A} = \int_{x \in X} \mu_{\tilde{A}}(x) / x = \int_{x \in X} \left(\int_{u \in [0,1]} \frac{1}{u} \right) / x \tag{6}$$

The membership function of IT2FLC is different from that of T1FLC. As shown in Figure 3, the value of the main membership function (MF) on the two-dimensional plane is an area (shaded area), which is contained by LMF (Lower Membership Function) and UMF (Upper Membership Function) and is called FOU (Footprint of Uncertainty). LMF and UMF are represented by $\underline{\mu}_{\tilde{A}}(x)$ and $\overline{\mu}_{\tilde{A}}(x)$, respectively, so \tilde{A} can also be expressed as

$$\tilde{A} = \int_{x \in X} \left[\underline{\mu}_{\tilde{A}}(x), \overline{\mu}_{\tilde{A}}(x) \right] / x \tag{7}$$

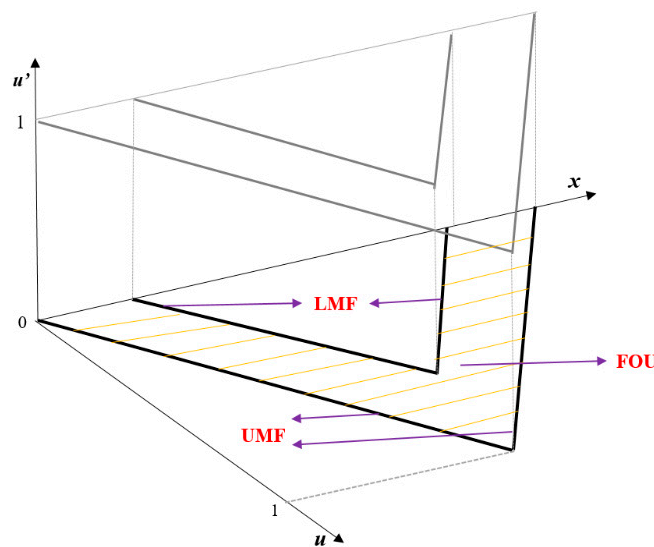


Figure 3. The type-2 membership function.

The introduction of FOU can include the uncertainties in the input of the system, so IT2FLC has a stronger ability to handle uncertainties.

Figure 4 shows the structure of IT2FLC. Compared with T1FLC, there is one more step: type reduction. Its function is to convert the T2FS output by fuzzy inference into T1FS, and then perform defuzzification calculation. Other processes are similar to T1FLC.

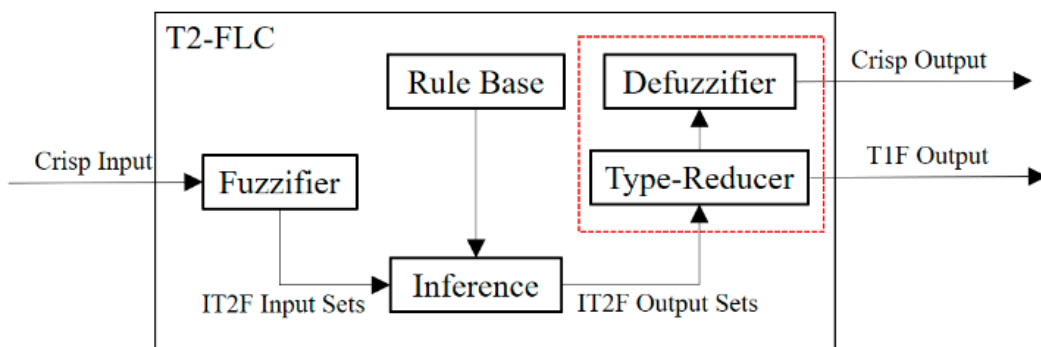


Figure 4. The T2FLC structure.

The fuzzy rule (FR) is expressed by Equation (8):

$$R^l : \text{IF } x_1 \text{ is } \tilde{X}_1^l \text{ and } \dots \text{ and } x_p \text{ is } \tilde{X}_p^l, \text{ THEN } y_l \text{ is } \tilde{Y}^l, l = 1, \dots, M \quad (8)$$

The activation intensity of the l rule is calculated by Equation (9):

$$F^l = \left[\underline{\mu_{\tilde{A}}(x_1)} \times \dots \times \underline{\mu_{\tilde{A}}(x_p)}, \overline{\mu_{\tilde{A}}(x_1)} \times \dots \times \overline{\mu_{\tilde{A}}(x_p)} \right] = \left[\underline{f^l}, \overline{f^l} \right] \quad (9)$$

The most commonly used center-of-gravity (COG) method reducer is shown in Equation (10):

$$Y_{\text{COG}} = \cup_{f^n \in F^n, y_n \in Y_n} \frac{\sum_{n=1}^N f^n y_n}{\sum_{n=1}^N f^n} = [y_l, y_r], \quad (10)$$

where y_l, y_r can be obtained by the TR algorithm, and the final defuzzification obtains the output of IT2FLC as

$$y = \frac{y_l + y_r}{2} \quad (11)$$

2.2.2. The Principle of FLC Realizes DHTC Technology

According to the introduction in Part 2 of this article, FLC can solve the two problems of DHTC.

For Question 1: As shown in Figure 3, the input of FLC is a range. By setting a reasonable membership function, a weight can be set for each precise value in the input range. We take the e and Δe of the photoelectric tracking system as the input of the FLC, set up reasonable fuzzy rules, and let the FLC determine the timing of switching.

For Question 2: Use the output value of FLC as the gain of the integrator. In the same way, by setting a reasonable membership function, the output value of the fuzzy controller is set to a gradual change, and the traditional "0" and "1" switch structure is changed to an integrator gain gradual change structure, which can avoid the shock caused by hard switching. When the fuzzy output is 0, the integrator is disconnected to realize the dynamic switching type.

2.3. WTNT TR Algorithm

Since the input membership function of IT2FLC is type-2, we need to transform T2-FS into T1-FS after the fuzzy inference to get the accurate output. Commonly used TR methods include KM, EKM, IASC, EIASC, etc., based on iterative convergence, which has the advantage of high calculation accuracy, but the disadvantage is slow calculation speed. There is also a kind of direct TR method without iteration, such as NT, BMM, UB algorithm, etc., which has the advantage of fast calculation speed, but in some cases, it is difficult to guarantee the accuracy of the degradation. The WEKM algorithm proposed by Mendel et al. is based on numerical integration to perform the weighted calculation of EKM. After simulation comparison, the calculation accuracy can be improved without affecting the speed [30]; based on Mendel research, CHEN et al. proposed GT2 FLS' WNT TR method; it is proved through simulation that the combination of numerical integration method with NT algorithm can also effectively improve the accuracy of the fuzzy defuzzification [31–33]. This provided inspiration to the author and constructed the WTNT reduction algorithm based on the compound trapezoidal rule in IT2FLC and applied it to the physical experimental system for the first time.

2.3.1. NT and CNT

The most recent studies on the type-reduction of interval type-2 fuzzy set have shown that the continuous version of NT (CNT) algorithms is an accurate method for defuzzifying [34]. Intuitively, we can feel that if the sampling size approaches infinity, random sampling will become an accurate TR method. The proof is as follows.

Theorem 1. When the number sampling is infinite, the random sampling algorithm will calculate the accurate centroid of IT2FS.

Proof Theorem 1. Suppose there is a discrete IT2FS \tilde{A} , whose domain is X . Let M represent the number of vertical slices along the y -axis, and L represents the number of horizontal slices along the μ -axis. Therefore, the total number of T1FS embedded in \tilde{A} is LM , because T1FS contains M vertical slices [35].

Let $\overline{\mu_{\tilde{A}}(x)}$ and $\underline{\mu_{\tilde{A}}(x)}$ denote the LMF and UMF of FOU, respectively. Select N embedded T1FS of \tilde{A} randomly. Let $\mu_i(x)$ be the MF of the i -th embedding set. Then, we summarized N randomly embedded T1-FS,

$$\sum_{i=1}^N \mu_i(x) = \sum_{j=1}^M \sum_{i=1}^N \mu_i(x_j) \tag{12}$$

Hence,

$$\lim_{N \rightarrow \infty} \frac{1}{N} \sum_{i=1}^N \mu_i(x) = \lim_{N \rightarrow \infty} \frac{1}{N} \sum_{j=1}^M \sum_{i=1}^N \mu_i(x_j) \tag{13}$$

Since $\mu_i(x_j)$ is a random value uniformly distributed on $[\underline{\mu_{\tilde{A}}(x)}, \overline{\mu_{\tilde{A}}(x)}]$, the right side of the equation can be transformed into

$$\lim_{N \rightarrow \infty} \frac{1}{N} \sum_{j=1}^M \sum_{i=1}^N \mu_i(x_j) = \frac{1}{L} \sum_{j=1}^M \sum_{k=1}^L \mu_k(x_j) \tag{14}$$

Hence,

$$\lim_{N \rightarrow \infty} \frac{L}{N} \sum_{i=1}^N \mu_i(x) = \sum_{j=1}^M \sum_{k=1}^L \mu_k(x_j) \tag{15}$$

For Equation (14), the left side is a random sampling of $N \rightarrow \infty$, and the right side is exactly the set of all \tilde{A} embedded MFs. Note that, since $\frac{L}{N}$ is only a constant, it does not affect calculating the centroid of \tilde{A} .

When \tilde{A} is a continuous IT2FS form, it is easy to get Equation (15) by replacing integral with summation

$$\lim_{N \rightarrow \infty} \frac{L}{N} \sum_{i=1}^N \mu_i(x) = \sum_{j=1}^M \sum_{k=1}^L \mu_k(x_j) \tag{16}$$

End of proof. \square

Therefore, when the step size of random sampling satisfies certain conditions, the NT algorithm in the discrete domain approximates the CNT algorithm, which is sufficient to meet the accuracy of the reduction.

2.3.2. Newton–Cotes Quadrature Formulas

Applying the Newton–Cotes formula, the definite integral of $f(x)$ in the interval $[a, b]$ can be estimated by using a limited number of sampling points. This provides a mathematical basis for the WTNT method through systematic sampling.

Definition 1 . (Numerical Integration) Suppose that $a = x_0 < x_1 < \dots < x_n = b$, then the following form of formula

$$Q(f) = \sum_{k=0}^m \omega_k f(x_k) = \omega_0 f(w_0) + \omega_1 f(w_1) + \dots + \omega_m f(w_m), \tag{17}$$

Which satisfies:

$$\int_a^b f(x)dx = Q(f) + E(f) \tag{18}$$

Then the above equation is called numerical integration or quadrature formula, where x_k is the integration node, ω_k is the weight coefficient, and $E(f)$ is the truncation error, that is, the error term of the integration formula.

Theorem 2. (Compound Trapezoidal Rule) Consider the function $y = f(x)$ on the closed interval $[a, b]$, and divide $[a, b]$ into m subintervals with a width of $h = \frac{b-a}{m}$, where the equidistant node is $x_k = x_0 + kh(k = 0, 1, \dots, m)$, then the numerical estimation of definite integral with the composite trapezoidal rule is as

$$\int_a^b f(x)dx = \frac{h}{2} \left(f(a) + f(b) + 2 \sum_{k=1}^{m-1} f(x_k) \right) + E_T(f, h) \tag{19}$$

If the function f is second-order continuous and differentiable on $[a, b]$, then the remainder

$$E_T(f, h) = -\frac{(b-a)f''(\zeta)}{12}h^2 = O(h^2) \tag{20}$$

where $a < \zeta < b$. $O(h^2)$ means that when the calculation step size is reduced by 1/2, the error should be reduced to $(1/2)^2 = 0.25$ times. That means that when the sampling step is smaller, the estimation error is smaller, which is sufficient to meet the accuracy requirements.

2.3.3. WTNT TR Algorithm

The classic NT algorithm was proposed by Nie and Tan [26]. It does not require iterative calculations, such as EM, which greatly simplifies the computational complexity and is more suitable for real-time systems. The NT algorithm is as Equation (21), and the calculated y_l, y_r are used in Equation (11) to calculate the exact value of fuzzy output.

$$y_l = \frac{\sum_{j=1}^N \underline{f^j} y_j}{\sum_{j=1}^N (\underline{f^j} + \overline{f^j})}; y_r = \frac{\sum_{j=1}^N \overline{f^j} y_j}{\sum_{j=1}^N (\underline{f^j} + \overline{f^j})} \tag{21}$$

Through the discussion of Theorems 1 and 2, it can be concluded that the NT algorithm in the discrete domain can meet the accuracy requirements of the defuzzification. Set $a = y_1 < y_2 < \dots < y_N = b$, construct the WTNT TR algorithm

$$y_l = \frac{\sum_{j=1}^N \omega_j \underline{f^j} y_j}{\sum_{j=1}^N \omega_j (\underline{f^j} + \overline{f^j})}; y_r = \frac{\sum_{j=1}^N \omega_j \overline{f^j} y_j}{\sum_{j=1}^N \omega_j (\underline{f^j} + \overline{f^j})} \tag{22}$$

where ω_j is the weighting coefficient, which is positioned as $\omega_j = \frac{1}{2}$ (if $j = 1, N$); $\omega_j = 1$ (if $j \neq 1, N$) according to the compound trapezoidal rule.

Based on the principle of numerical integration, the WTNT algorithm can theoretically approximate the CNT algorithm, which is more accurate than the NT algorithm. In fact, the NT algorithm is only a special case of the WTNT algorithm when $\omega_j = 1$ ($j = 1, 2, \dots, N$). Since the output of the IT2FLC set in this paper is discretized, it is not necessary to discuss the reduction of the continuous domain as in the literature [28,29], which simplifies the calculation. The sampling step is determined by fuzzy rules, rather than artificial settings.

the steady-state range, the access of the integrator should be avoided as much as possible; because there is noise in the actual system, its Δe is irregular. In this case, it is easy to connect the integrator and cause the system to deviate from the balanced position again. When e is in P and N state, it is the best time to connect the integrator, which can achieve a significant correction effect under the premise of system stability. Finally, the mechanism for determining type switching is shown in Figure 7, when e and Δe are in six states in the figure:

- State 1: e is P, Δe is PB, and e will continue to increase. At this time, the integrator should be connected to intervene to make the output k value of FLC be PB so that the system can quickly return to the reference value.
- State 2: e is PB, Δe is P. To prevent integral saturation, disconnect the integrator.
- State 3: e is PB, Δe is Z. The system is about to approach the equilibrium position, and the integrator should be connected to speed up the response.
- State 4: e is PB, and Δe is N. The system approaches the equilibrium position at a faster speed. At this time, the integrator can be properly connected, but the gain cannot be too large.
- State 5: e is P and Δe is NB. It is safer to connect to the integrator in this situation.
- State 6: e is Z. As mentioned earlier, the integrator should be disconnected to prevent the system from deviating from the equilibrium position.
- Similarly, the same judgment mechanism is used when e is N and NB. Therefore, set the fuzzy rules of T1FLC as shown in Table 1.

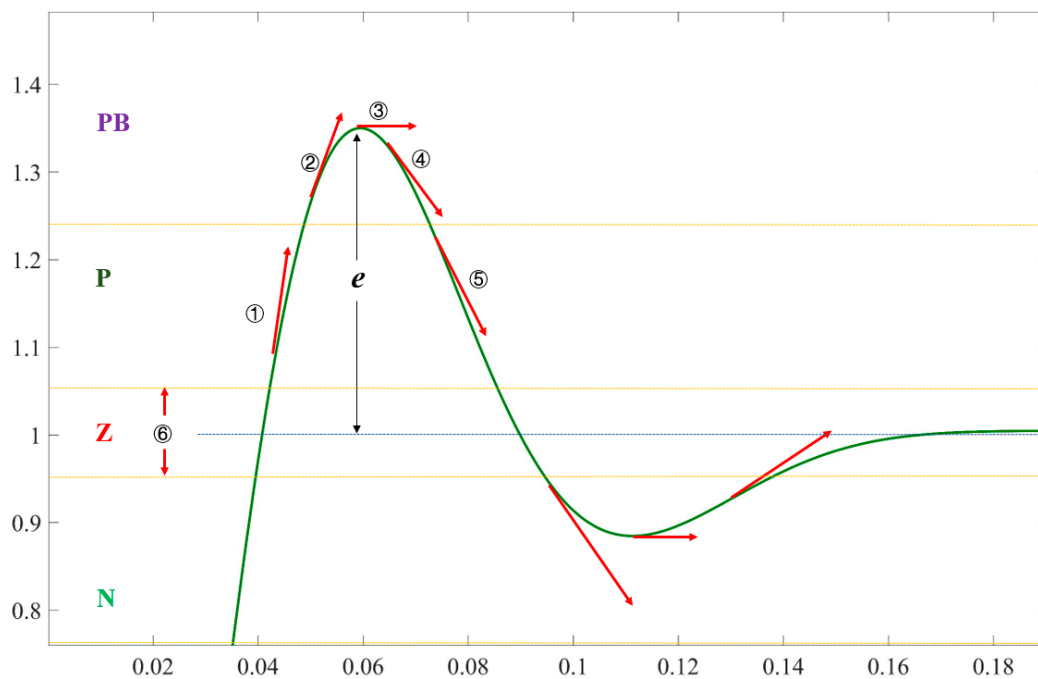


Figure 7. The judgment mechanism of type switching.

Table 1. The rule base ¹.

	Rules	e				
		NB	N	Z	P	PB
Δe	NB	NB	NB	NB	PB	NB
	N	NB	N	NB	P	N
	Z	Z	Z	NB	Z	Z
	P	N	P	NB	N	NB
	PB	NB	PB	NB	NB	NB

¹ The dark blue font in the table is FLC output k.

3. The defuzzification uses the COG method:

$$y_{COG} = \frac{\sum_{l=1}^M y_l \mu_A^l(y_l)}{\sum_{l=1}^N \mu_A^l(y_l)} \tag{23}$$

3.2. IT2FLC Settings

The MF setting is shown in Figure 8. Since the membership function of IT2FLC is two-dimensional, the calculation complexity is relatively high. To speed up the calculation, we reduce the number of language variables. From the experimental comparison, the calculation accuracy can still meet actual needs. Set three language variables N, Z, P for e and Δe , and each variable has upper and lower bounds. The output variable k follows the form of T1FLC.

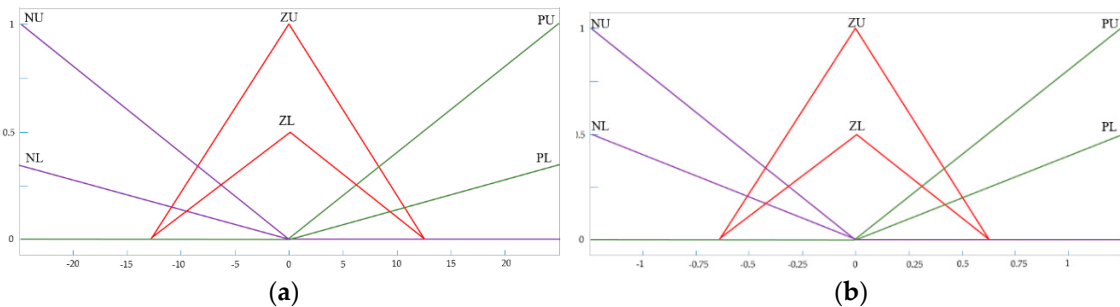


Figure 8. The IT2FLC membership function (MF): (a) MF of ‘e’; (b) MF of ‘ Δe ’.

The design of the fuzzy rule library follows the principle of T1FLC, but the number of rules is changed from 5×5 to 3×3 , as shown in the dotted box in Table 1.

The reduction algorithm selects WTNT, EKM, and EIASC for comparison.

3.3. MPGA Design

3.3.1. MPGA Advantages

As Figure 9 shows, the MPGA is constructed based on the coding, selection, crossover, and mutation of the standard genetic algorithm (SGA) which adds an immigration operator and multiple populations. MPGA breaks through the framework of SGA that only relies on a single population for genetic evolution, introducing multiple populations for simultaneous optimization searches. Different populations are assigned different crossover and mutation probabilities, taking into account global and local search performance. The various populations are connected through the migration operator, and its function is to replace the best value of the former group with the worst quality of the latter group to realize the co-evolution of multiple groups. The best individuals in each evolutionary generation of various groups are preserved by manual selection operators to form the elite populations. The elite populations do not perform selection, crossover, mutation, and other genetic operations to ensure that the best individuals generated by various groups are not destroyed or lost during the evolution process. At the same time, the elite populations are

also the basis for judging the termination of the algorithm. In MPGA, the minimum algebra of the optimal individual is used as the termination criterion. This criterion makes full use of the knowledge accumulation of the genetic algorithm in the evolution process and is more reasonable than the maximum genetic algebra criterion [36,37].

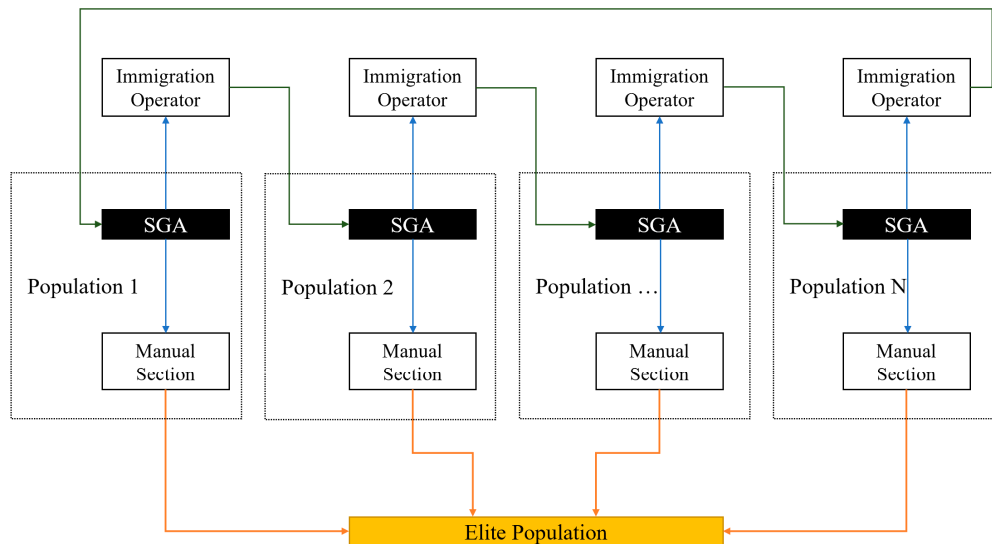


Figure 9. The MPGA structure.

3.3.2. MPGA Design Process

Determine the Optimized Parameters

There are many ways to optimize FLC with GA, which can optimize parameters, such as rule base, membership function, scale factor, and so on. Through experimental comparison, it is found that the optimization rule base or membership function has a large amount of calculation, complex parameter settings, and low efficiency; the optimization scale factor is simple, the calculation speed is fast, and it is convenient to modify. Therefore, this project keeps the rule base and membership function unchanged and uses the three scaling factors K_e , K_{ec} , and K_u (Figure 5) as the parameters to optimize the chromosome coding.

The larger the K_e value, the faster the step response, but at the same time, the overshoot and adjustment time will increase, and even the system will not work steadily. Contrary to the K_e effect, the smaller the K_{ec} , the larger the overshoot and adjustment time. K_u corresponds to the total magnification of the system. Generally, K_u increases and the rise speed is faster, but when K_u is too large, it will produce a larger overshoot which affects the steady-state operation.

Therefore, using MPGA to optimize three parameters at the same time can give full play to the advantages of global search and find the optimal solution of the three parameters.

Determine the Fitness Function

The GA does not use external information in the optimization search. It only uses the fitness function as the basis and uses the fitness value of each individual in the population to search. In the control system, our commonly used objective function is the integral error criterion (ITAE):

$$J(ITAE) = \int_0^{\infty} t \cdot |e(t)| dt, \quad (24)$$

where t is the running time of the system, and $|e(t)|$ is the absolute value of the system error. The smaller the ITAE value, the better the performance. It can comprehensively evaluate the control system's response time, overshoot, and other dynamic and static performance. Since the genetic operation is carried out according to the size of the fitness value, and the optimization direction of the objective function should correspond to the direction in which

the fitness value increases, the performance index function is appropriately transformed to obtain the fitness function:

$$f = \frac{1}{1 + J(ITAE)} \quad (25)$$

Determine the Operating Parameters of the Genetic Algorithm

Operating parameters include population size M , population number N , optimal individual minimum retention algebra MAXGEN, elite population ratio ELITE, mutation probability P_m , crossover probability P_c , etc. Among them, the population size, number, and the minimum number of optimal individuals have the greatest impact on the results and calculation time. If it is too small, the optimization result is not ideal, and if it is too large, the iteration will take more time. The mutation probability and the crossover probability determine the system's global and local search capabilities. When they are larger, the recombined individuals will have a high probability of appearing and converge quickly; but at the same time, the replacement of the old and the new is too fast, making some superior individuals may be eliminated prematurely [38–40].

In this project, the MPGA parameters are set as $M = 20$, $N = 10$, MAXGEN = 10, ELITE = 20%, P_m is a random number between 0.7–0.9, P_c is a random number between 0.001–0.05, and different populations take different probabilities to prevent precocity.

4. Experimental Verification

On the flexible fast steering mirror (FFSM) experimental platform, the control effects of C_p , T1FLC, and IT2FLC were verified, respectively, and the advantages and disadvantages of the control effects were compared from the four aspects of step response adjustment time, steady-state error, mean square error, and ITAE index. To verify the ability of IT2FLC to deal with uncertainties, three repeated experiments were performed on three control controllers for comparison. In addition, NT, EKM, and EIASC are selected to compare the effects of IT2FLC, and the best TR algorithm in the real-time control system is obtained.

4.1. Experimental Platform Characteristics and C_p Design

As shown in Figure 10, the FFSM experiment platform consists of an adjustable base, a flexible mirror, a voice coil motor, a position sensor, a control cabinet, and a communication bus. By adjusting the adjustable base, different characteristics of the controlled object can be obtained. The flexible mirror is driven by a voice coil motor to track the reference input signal. The mirror is made of metal with softer material properties, and it will be slightly deformed during the movement, which will bring uncertainties to the system. The position sensor outputs the mirror position in real time. The communication bus is responsible for the signal transmission, and the control cabinet implements the control operation.

Through frequency sweep processing, the model of the controlled object is obtained. The transfer function $G_0(s)$ (Equation (26)) consists of two second-order oscillation elements (SOOE), one second-order differentiation element (SODE), one first-order inertial element (FOIE), and a delay element (DE). The data in Table 2 are obtained after identification. The identification effect comparison is shown in Figure 11a.

Table 2. Identification parameters ².

	SOOE 1	SOOE 2	SODE	FOIE	DE
ω	241.9026	333.0088	282.7433	-	-
ζ	0.228	0.165	0.220	-	-
others	-	-	-	$T_0 = 0.0005$	$T_1 = 0.0003$

² ω is the angular frequency, ζ is the damping constant, others represent other parameters.

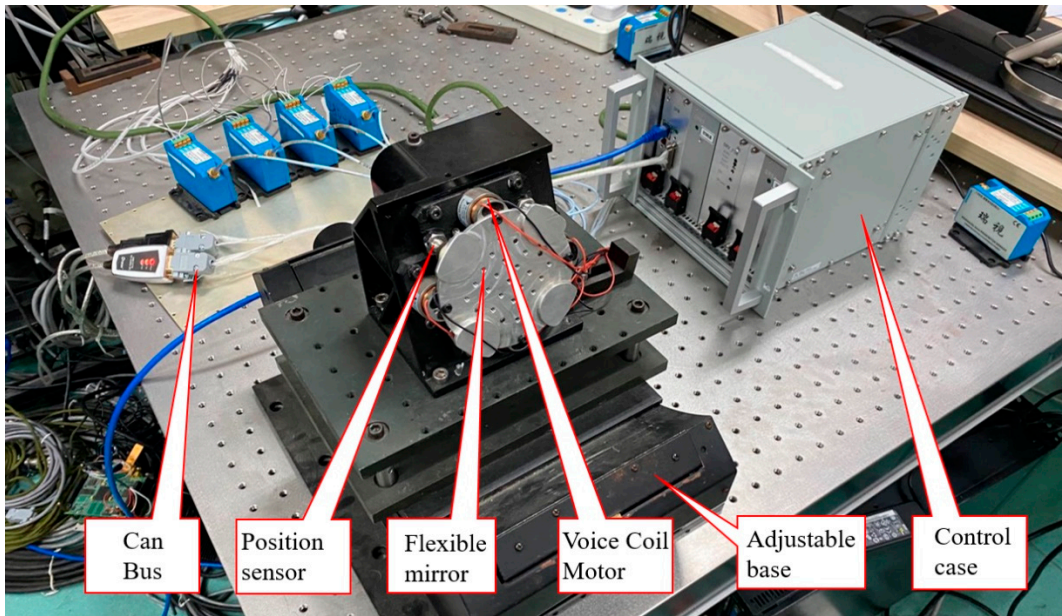


Figure 10. The FFSM experiment platform.

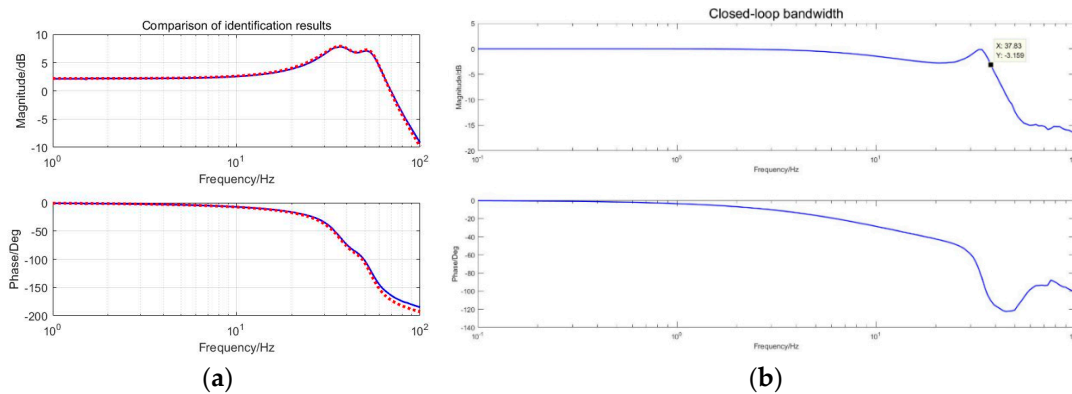


Figure 11. Identification results: (a) Comparison of identification results; (b) Closed-loop bandwidth.

The position controller C_p is designed with a simple and practical zero-pole cancellation method. The open-loop transfer function of the forward path $G_{cp}(s)$ is obtained as Equation (27).

The measured closed-loop bandwidth under C_p control is 37.83 Hz (Figure 11b), which meets the bandwidth requirements under actual application conditions.

$$G_0(s) = k * \frac{\left(\frac{s}{w_3}\right)^2 + \frac{2\zeta_3}{w_3}s + 1}{\left(\left(\frac{s}{w_1}\right)^2 + \frac{2\zeta_1}{w_1}s + 1\right)\left(\left(\frac{s}{w_2}\right)^2 + \frac{2\zeta_2}{w_2}s + 1\right)(T_0s + 1)} * e^{-T_1s} \quad (26)$$

$$G_{cp}(s) = K * \frac{1}{(T_0s + 1) \cdot s} * e^{-T_1s} \quad (27)$$

4.2. C_p and T_1 and T_2 Step Response Comparison

In the experimental platform, C_p , T_1 FLC, and T_2 FLC are used for step response experiments. Figure 12 shows the comparison of the response curves of the three control modes. Table 3 shows the settling time (TS), steady-state error (ESS), variance (VAR), and ITAE value of each mode. It can be seen that in the FLC control mode, the four aspects of

TS, ESS, VAR, and ITAE index are better than the system with only Cp. T2FLC is better than T1FLC, which reaches a stable state faster and has the least jitter.

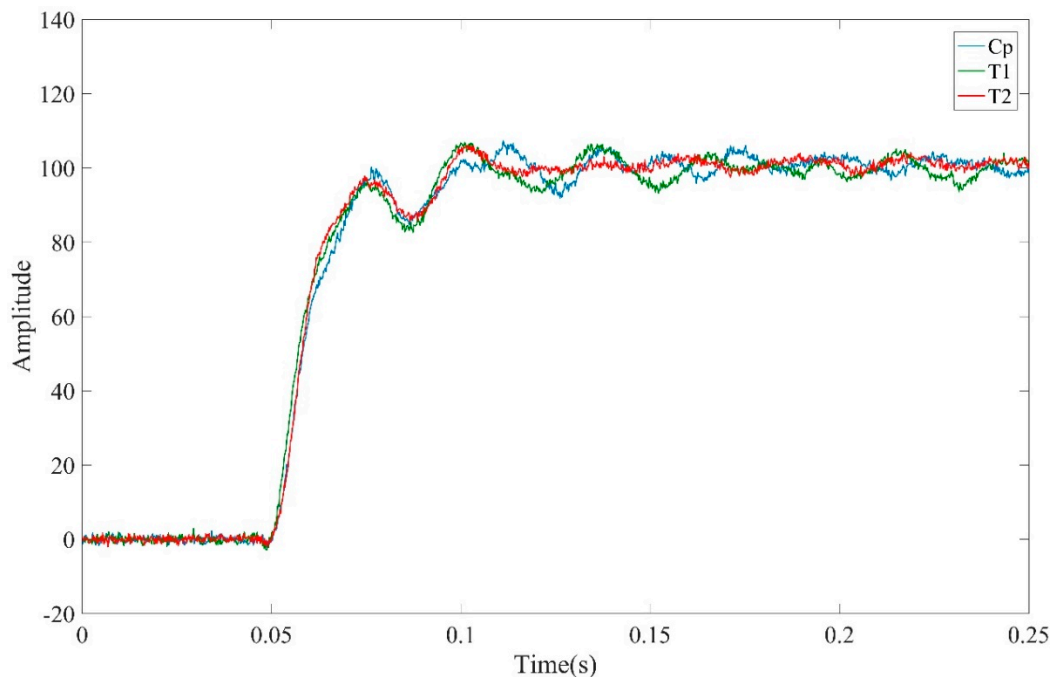


Figure 12. Cp and T1 and T2 step response comparison.

Table 3. Cp and T1 and T2 step response comparison.

	TS	ESS	VAR	J(ITAE)
CP	0.136	0.3083	1.6174	1251.8
T1	0.120	0.0031	1.3003	1200.9
T2	0.069	0.0005	1.2038	979.6

It can be seen from Figure 13 that under the guidance of the fuzzy rules when the system starts a step response, the output of the FLC changes accordingly, so the output of the integrator changes accordingly, and the system type changes dynamically. The step output curve quickly reached a stable state, indicating that the FLC access is effective and the goal of dynamically changing the type has been achieved.

4.3. Comparison of the Ability to Handle Uncertainties

Next, compare the uncertainties performance of each control mode. The uncertainties of the experimental platform mainly come from the following aspects:

- The flexible mirror will be slightly deformed during the movement, resulting in uncertain position output.
- The friction between shaft systems and the characteristics of motor output brings uncertainties.
- The uncertainties are caused by environmental noise and mechanical noise.

Figure 14a and Table 4 show the step response state in the mode of Cp only. In the case of the same control parameters, the shape of the step response curve is quite different, and the indicators are also very different, which shows that the Cp has a poor ability to handle uncertainties.

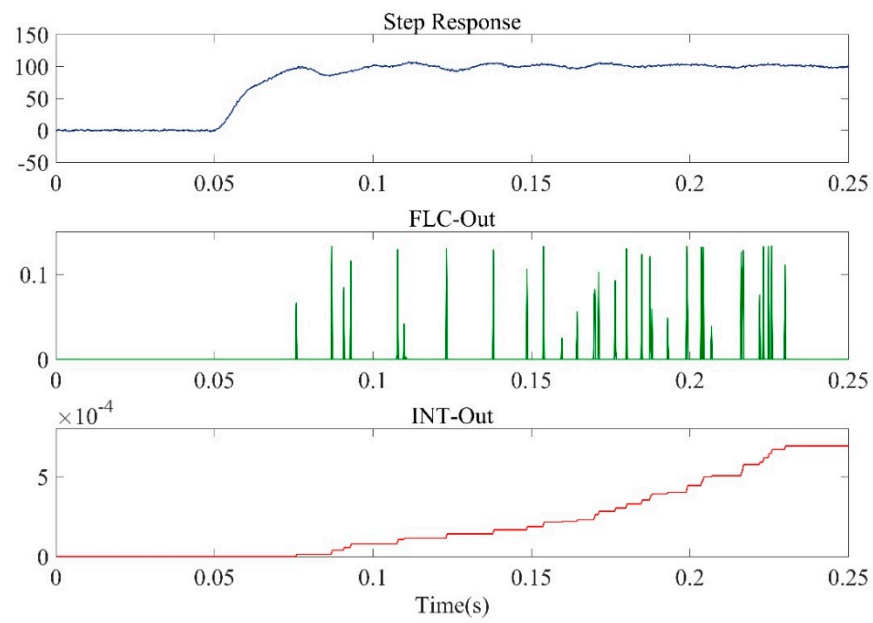


Figure 13. FLC dynamic response.

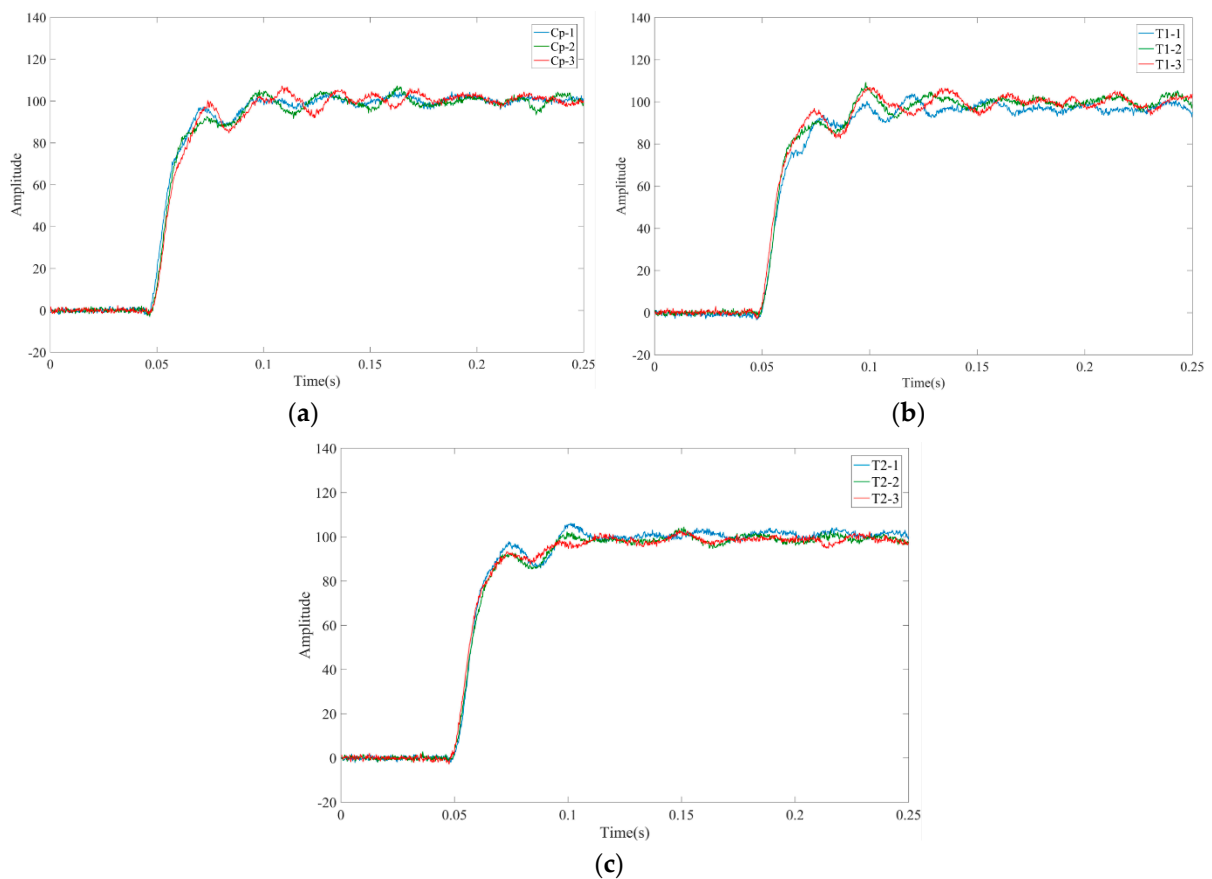


Figure 14. Comparison of three experiments with the same parameters in (a) Cp mode; (b) T1FLC mode; (c) IT2FLC mode.

Table 4. Three experiments comparison in Cp mode.

	TS	ESS	VAR	J(ITAE)
CP-1	0.1046	0.0049	3.0578	1164.6
CP-2	0.1426	1.0235	1.0406	1090.9
CP-3	0.1358	0.3083	1.6174	1251.8

Figure 14b and Table 5 show the step response under the T1FLC mode. Its various indicators are more stable and better than the Cp mode, but the dynamic curve shape is still quite different.

Table 5. Three experiments comparison in T1FLC mode.

	TS	ESS	VAR	J(ITAE)
T1-1	0.1024	0.0152	1.0506	875.1
T1-2	0.1016	0.0054	1.6502	1362.6
T1-3	0.1107	0.0031	1.3003	1191.1

Figure 14c and Table 6 show the step response in T2FLC control mode. The dynamic curve shape difference is small, the steady-state error is reduced to 4 decimal places, and the fluctuation range is not large. In addition, the steady-state accuracy is improved, the adjustment time can be maintained at 2 decimal places, and VAR and ITAE values keep within a small fluctuation range, which is more excellent than the other two control modes.

Table 6. Three experiments comparison in IT2FLC mode.

	TS	ESS	VAR	J(ITAE)
T2-1	0.0548	0.0005	1.2038	974.5
T2-2	0.0496	0.0096	1.4572	885.1
T2-3	0.0598	0.0081	1.1244	1105.0

In summary, IT2FLC can better handle system uncertainties than Cp and T1FLC.

4.4. Comparison of TR Algorithms

Figure 15 and Table 7 are comparisons of the three TR algorithms of NT, WTNT, EKM, and EIASC. EKM and EIASC apply the principle of iterative optimization to find the optimal solution, which is more complicated than the WTNT algorithm. From the response results, under the same parameters, both NT, WTNT, and EKM can ensure the stability of the system, but EKM will bring greater jitter, and the values of VAR and ITAE are large and unstable, while EIASC diverges the step response and does not apply to this experimental platform. Comparing NT and WTNT, we can see that the WTNT algorithm has a faster response speed and higher steady-state accuracy. Meanwhile, the VAR and ITAE values of WTNT are smaller than NT, indicating that the WTNT algorithm has stronger robustness.

Table 7. Comparison of three TR algorithms.

	TS	ESS	VAR	J(ITAE)
WTNT	0.06	0.0005	1.2038	981.2
NT	0.13	0.0096	1.4572	1102.4
EKM	Oscillating	0.0039	29.774	1832.3
EIASC	Divergence	5.8521	3.1872	1409.6

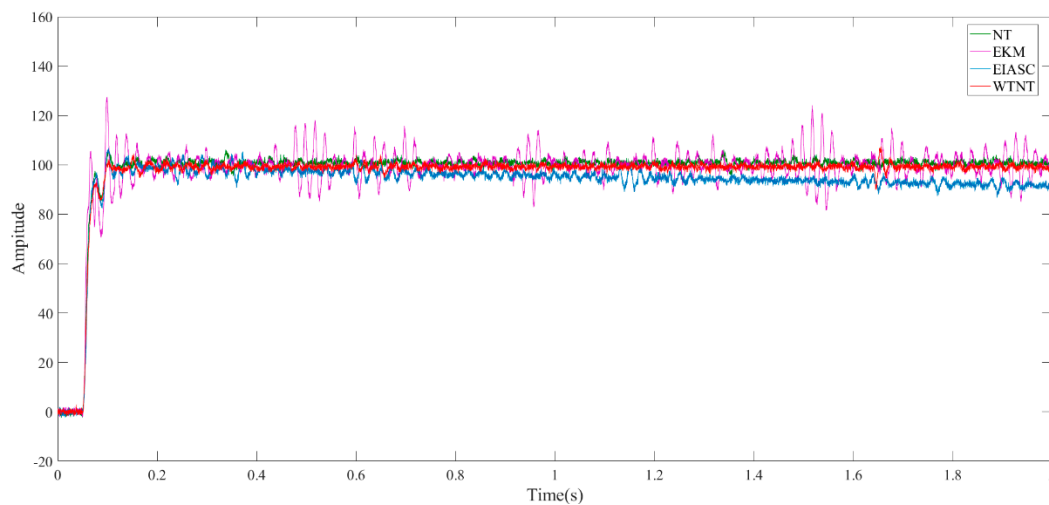


Figure 15. Comparison of three TR algorithms.

On the whole, for this experimental platform, the WTNT algorithm results are the best, and the algorithm itself does not require iteration, the calculation speed is the fastest, and it is more suitable for real-time control systems.

5. Conclusions

A IT2FLC-DHTC is constructed and verified in an FFSM platform. On the premise of ensuring the stability of the system, the dynamic and steady-state performance is improved, and the goal of dynamic high-type control is achieved.

Adding an integrator to a traditional closed-loop control system can effectively improve the steady-state accuracy of the system. However, the increase of integrators will aggravate the oscillation of the system. In order to avoid system divergence, a dynamic adjustment mechanism is introduced to change the number of integrators with the state of the system, that is, the type of the system. From the experimental results, the dynamic high-type controller can effectively improve the steady-state accuracy of the system while avoiding the system oscillation.

Compared with traditional position controllers, fuzzy logic controller shows great advantages in handling uncertainties, which benefits from the inherent characteristics of FLC. In this paper, a FLC is introduced as the on-off switch of the integrator, and also control the gain of the integrator. By reasonably designing the fuzzy rule base and membership function, the FLC can adjust the on-off and gain of the integrator in real time according to the system state, which effectively improves the system's response speed, steady-state accuracy, and ability to handle uncertainties.

IT2FLC introduces a three-dimensional membership function, which further improves the fuzzy controller's ability to handle uncertainties. From the experimental results, compared with T1FLC, IT2FLC's ability to handle uncertainties is significantly improved. In addition, in order to speed up the calculation speed of IT2FLC, the WTNT type-reduction algorithm constructed in this paper has faster calculation speed and better steady-state accuracy than the traditional TR algorithm, and has been successfully applied to real-time control systems, with good engineering application value.

Future work will continue on the combination of FLC and DHTC. DHTC is a relatively new field. The current mainstream control structure type does not exceed type-3, and the combination of FLC and DHTC does not exceed type-2. If the type can be broken to a higher level, the steady-state accuracy of the system can undoubtedly be further improved, which has important research significance in the engineering field that requires high precision. In addition, the research of the type-2 FLC is also in the preliminary stage, the application field is almost blank, and there are many worthy research areas waiting for us to explore. I believe that in the near future, fuzzy control and high-type control can shine in the field of control, let us wait and see.

Author Contributions: Conceptualization, S.Q., T.Z. and Y.M.; Data curation, S.Q.; Formal analysis, S.Q. and T.Z.; Funding acquisition, Q.B.; Investigation, S.Q. and Q.B.; Methodology, S.Q. and Y.M.; Software, W.T.; Supervision, C.Z.; Validation, C.Z.; Writing – original draft, S.Q.; Writing—review & editing, S.Q., C.Z. and Y.M. All authors have read and agreed to the published version of the manuscript.

Funding: The APC was funded by Institute of Optics and Electrics, Chinese Academy of Sciences, China.

Institutional Review Board Statement: Not applicable.

Informed Consent Statement: Not applicable.

Data Availability Statement: Not applicable.

Conflicts of Interest: The authors declare no conflict of interest.

References

1. Tang, T.; Ma, J.; Ren, G. PID-I controller of charge coupled device-based tracking loop for fast-steering mirror. *Opt. Eng.* **2011**, *50*, 043002. [[CrossRef](#)]
2. Portillo, A.A.; Ortiz, G.G.; Racho, C. Fine pointing control for optical communications. In Proceedings of the 2001 IEEE Aerospace Conference, Big Sky, MT, USA, 10–17 March 2001; pp. 1541–1550.
3. Zhong, J.; Li, L.; Nishida, R.; Shinshi, T. Design and evaluation of a PEA-driven fast steering mirror with a permanent magnet preload force mechanism. *Precis. Eng.* **2020**, *62*, 95–105. [[CrossRef](#)]
4. Budiharto, W.; Irwansyah, E.; Suroso, J.S.; Gunawan, A.A.S. Design of object tracking for military robot using PID controller and computer vision. *ICIC Express Lett.* **2020**, *14*, 289–294.
5. Kim, D.H.; Nguyen, T.H.; Pratama, P.S.; Kim, H.K.; Jung, Y.S.; Kim, S.B. Servo system design for speed control of AC induction motors using polynomial differential operator. *Int. J. Control Autom. Syst.* **2017**, *15*, 1207–1216. [[CrossRef](#)]
6. Nazari, V.; Surgenor, B. Improved position tracking performance of a pneumatic actuator using a fuzzy logic controller with velocity, system lag and friction compensation. *Int. J. Control Autom. Syst.* **2016**, *14*, 1376–1388. [[CrossRef](#)]
7. Abdulkhader, H.K.; Jacob, J.; Mathew, A.T. Fractional-order lead-lag compensator-based multi-band power system stabiliser design using a hybrid dynamic GA-PSO algorithm. *IET Gener. Transm. Distrib.* **2018**, *12*, 3248–3260. [[CrossRef](#)]
8. Deng, C.; Tang, T.; Mao, Y.; Ren, G. Enhanced Disturbance Observer Based on Acceleration Measurement for Fast Steering Mirror Systems. *IEEE Photon-J.* **2017**, *9*, 1–11.
9. Ding, X.; Li, R.; Cheng, Y.; Liu, Q.; Liu, J. Design of and Research into a Multiple-Fuzzy PID Suspension Control System Based on Road Recognition. *Processes* **2021**, *9*, 2190. [[CrossRef](#)]
10. Bradley, L.M.; Corriveau, J.P. Launch area theodolite system, Acquisition, Tracking, and Pointing. *V. Int. Soc. Opt. Photonics* **1991**, *1482*, 48–60.
11. KPapadopoulos, K.G.; Papastefanaki, E.N.; Margaris, N.I. Explicit Analytical PID Tuning Rules for the Design of Type-III Control Loops. *IEEE Trans. Ind. Electron.* **2012**, *60*, 4650–4664. [[CrossRef](#)]
12. Huang, J.-T.; Chiu, C.-K. Adaptive Fuzzy Sliding Mode Control of Omnidirectional Mobile Robots with Prescribed Performance. *Processes* **2021**, *9*, 2211. [[CrossRef](#)]
13. Youn, B.; Sun, D. Fuzzy PID control technology for synchronous generator excitation. *Int. J. Control Autom.* **2015**, *8*, 91–98. [[CrossRef](#)]
14. Wang, Y.; Ren, W.; Liu, Z.; Li, J.; Zhang, D. T-S Fuzzy Model-Based Fault Detection for Continuous Stirring Tank Reactor. *Processes* **2021**, *9*, 2127. [[CrossRef](#)]
15. Wang, X.; Zheng, G.; Ma, H.; Bai, W.; Wu, H.; Ji, B. Fuzzy Control-Based Energy-Aware Routing Protocol for Wireless Body Area Networks. *J. Sens.* **2021**, *2021*, 1–13. [[CrossRef](#)]
16. Zhu, A.; Ai, H.; Chen, L. A Fuzzy Logic Reinforcement Learning Control with Spring-Damper Device for Space Robot Capturing Satellite. *Appl. Sci.* **2022**, *12*, 2662. [[CrossRef](#)]
17. Wang, P.; Yang, J.; Zhang, X. Stability improvement in a gain-clamped L-band erbium-doped fiber amplifier through hybrid gain control. *Opt. Eng.* **2018**, *57*, 056105. [[CrossRef](#)]
18. Qin, S.; Bao, Q.; Duan, Q.; Mao, Y. Design of Opto-Electronic Tracking Servo System Based on Fuzzy II-order Control System. In Proceedings of the 2020 IEEE 4th Information Technology, Networking, Electronic and Automation Control Conference (ITNEC), Chongqing, China, 12–14 June 2020; Volume 1, pp. 1354–1360.
19. Karnik, N.N.; Mendel, J.M.; Liang, Q. Type-2 fuzzy logic system. *IEEE Trans. Fuzzy Syst.* **1999**, *7*, 643–658. [[CrossRef](#)]
20. Mendel, J.M.; John, R.I.B. Type-2 fuzzy sets made simple. *IEEE Trans. Fuzzy Syst.* **2002**, *10*, 117–127. [[CrossRef](#)]
21. Hagrass, H. Type-2 FLCs: A new generation of fuzzy controllers. *IEEE Comput. Intell. Mag.* **2007**, *2*, 30–43. [[CrossRef](#)]
22. Zadeh, L.A. The concept of a linguistic variable and its application to approximate reasoning—I. *Inf. Sci.* **1975**, *8*, 199–249. [[CrossRef](#)]

23. Hisdal, E. The IF THEN ELSE statement and interval-valued fuzzy sets of higher type. *Int. J. Man. Machine Stud.* **1981**, *15*, 385–455. [[CrossRef](#)]
24. Palacio-Morales, J.; Tobón, A.; Herrera, J. Optimization Based on Pattern Search Algorithm Applied to pH Non-Linear Control: Application to Alkalinization Process of Sugar Juice. *Processes* **2021**, *9*, 2283. [[CrossRef](#)]
25. Wu, D.; Nie, M. Comparison and practical implementation of type reduction algorithms for type-2 fuzzy sets and systems. In Proceedings of the 2011 IEEE International Conference on Fuzzy Systems, Taipei, Taiwan, 27–30 June 2011; pp. 2131–2138.
26. Firouzi, B.; Alattas, K.A.; Bakouri, M.; Alanazi, A.K.; Mohammadzadeh, A.; Mobayen, S.; Fekih, A. A Type-2 Fuzzy Controller for Floating Tension-Leg Platforms in Wind Turbines. *Energies* **2022**, *15*, 1705. [[CrossRef](#)]
27. Sibilska-Mroziewicz, A.; Ordys, A.; Możaryn, J.; Hosseinabadi, P.A.; Abadi, A.S.S.; Pota, H. LQR and Fuzzy Logic Control for the Three-Area Power System. *Energies* **2021**, *14*, 8522. [[CrossRef](#)]
28. Nie, M.; Tan, W.W. Towards an efficient type-reduction method for interval type-2 fuzzy logic systems. In Proceedings of the 2008 IEEE International Conference on Fuzzy Systems (IEEE World Congress on Computational Intelligence), Hong Kong, China, 1–6 June 2008; pp. 1425–1432.
29. Li, J.; John, R.; Coupland, S.; Kendall, G. On Nie-Tan Operator and Type-Reduction of Interval Type-2 Fuzzy Sets. *IEEE Trans. Fuzzy Syst.* **2017**, *26*, 1036–1039. [[CrossRef](#)]
30. Liu, X.; Mendel, J.M.; Wu, D. Study on enhanced Karnik–Mendel algorithms: Initialization explanations and computation improvements. *Inf. Sci.* **2012**, *184*, 75–91. [[CrossRef](#)]
31. Chen, Y.; Wang, D. Study on centroid type-reduction of general type-2 fuzzy logic systems with weighted Nie–Tan algorithms. *Soft Comput.* **2018**, *22*, 7659–7678. [[CrossRef](#)]
32. Šitum, Ž.; Ćorić, D. Position Control of a Pneumatic Drive Using a Fuzzy Controller with an Analytic Activation Function. *Sensors* **2022**, *22*, 1004. [[CrossRef](#)]
33. Lv, L.; Wang, J.; Long, J. Interval Type-2 Fuzzy Logic Anti-Lock Braking Control for Electric Vehicles under Complex Road Conditions. *Sustainability* **2021**, *13*, 11531. [[CrossRef](#)]
34. Zakaria, R.; Wahab, A.F.; Ismail, I.; Zulkifly, M.I.E. Complex Uncertainty of Surface Data Modeling via the Type-2 Fuzzy B-Spline Model. *Mathematics* **2021**, *9*, 1054. [[CrossRef](#)]
35. Ontiveros-Robles, E.; Melin, P.; Castillo, O. New Methodology to Approximate Type-Reduction Based on a Continuous Root-Finding Karnik Mendel Algorithm. *Algorithms* **2017**, *10*, 77. [[CrossRef](#)]
36. Fei, Y.U. Applying Multi-Population Genetic Algorithm To The Dynamic Flexible Job Shop Scheduling Problem. *Acad. J. Manuf. Eng.* **2020**, *18*, 37–42.
37. Van Veldhuizen, D.A.; Lamont, G.B. Multiobjective Evolutionary Algorithms: Analyzing the State-of-the-Art. *Evol. Comput.* **2000**, *8*, 125–147. [[CrossRef](#)] [[PubMed](#)]
38. Zhu, K.; Gu, C.; Qiu, J.; Liu, W.; Fang, C.; Li, B. Determining the Optimal Placement of Sensors on a Concrete Arch Dam Using a Quantum Genetic Algorithm. *J. Sens.* **2016**, *2016*, 1–10. [[CrossRef](#)]
39. Wang, L.; Zhai, Z.; Zhu, Z.; Mao, E. Path Tracking Control of an Autonomous Tractor Using Improved Stanley Controller Optimized with Multiple-Population Genetic Algorithm. *Actuators* **2022**, *11*, 22. [[CrossRef](#)]
40. Teng, D.; Li, Y.; Yang, H.; Wei, Z.; Li, Y. Genetic Algorithm for Sparse Optimization of Mills Cross Array Used in Underwater Acoustic Imaging. *J. Mar. Sci. Eng.* **2022**, *10*, 155. [[CrossRef](#)]